Superalloys 2012: 12th International Symposium on Superalloys
Edited by: Eric S. Huron, Roger C. Reed, Mark C. Hardy, Michael J. Mills, Rick E. Montero, Pedro D. Portella, Jack Telesman
TMS (The Minerals, Metals & Materials Society), 2012

EFFECTS OF Y AND La ADDITIONS ON THE PROCESSING AND PROPERTIES OF A SECOND GENERATION SINGLE CRYSTAL NICKEL-BASE SUPERALLOY CMSX-4®

H.T. Pang[1], I.M. Edmonds[2], C.N. Jones[2], H.J. Stone[1], C.M.F. Rae[1]
[1]Dept. of Materials Science and Metallurgy, University of Cambridge, Pembroke Street, Cambridge CB2 3QZ, United Kingdom.
[2]Rolls-Royce plc., P.O. Box 31, Derby DE24 8BJ, United Kingdom.

Keywords: Yttrium, Lanthanum, Solution Heat Treatment, Alloy Stability, TCP Phase

Abstract

The effects of yttrium and lanthanum additions on the processing and properties of a second generation single crystal nickel-base turbine blade superalloy CMSX-4® are investigated. The additions of Y and La at 20 ppm Y+La did not have a significant effect on the as-cast microstructure; while at 65 and 350 ppm, the appearance of Y and La-rich phases becomes increasingly apparent. The partitioning of the major alloying elements was unaltered by the rare-earth additions as shown by EPMA mapping carried out on as-cast samples. However, DSC studies indicate that the as-cast incipient melting temperatures were progressively lowered with increasing Y+La additions. Subsequent solution heat treatment trials therefore showed increased susceptibility to incipient melting for alloys with 65 and 350 ppm Y+La. Alloy stability studies carried out at 1000°C and 1100°C indicate increased propensity to TCP phases formation with Y+La additions of up to 65 ppm; while at 350 ppm Y+La, the occurrence of TCP phases appeared to decrease. It appears that the implementation of Y and La additions to single crystal turbine blades has to be carried out carefully to balance the improvements which may be obtained in oxidation/environmental protection performance against the potential issues related to processing e.g. solution heat treatment, and metallurgical issues such as alloy stability.

Introduction

Nickel-base single crystal superalloys have been the material of choice for turbine blade applications as they possess a good balance of the properties required for operation in the severe high temperature conditions. Due to the drive to improve aeroengine efficiency which could be achieved by higher engine operating temperatures, development of new generations of single crystal superalloys has primarily focused on additions of dense refractory elements to improve the temperature capabilities of these alloys, specifically the mechanical and environmental protection performance.

However, there is further scope for development of the current generation of alloys which possess sufficient mechanical properties, i.e., by the additions of trace rare-earth elements to improve the oxidation/environmental protection performance. This route of alloy development allows the lifecycles of current mature alloy systems to be extended. In addition, the service temperature of turbine blades made with these improved materials may be increased which allows for more economic operation.

Previous studies have shown trace rare earth additions of yttrium and lanthanum to be beneficial to the environmental protection performance of single crystal nickel-base alloys [1,2,3]. However, potential issues may arise during processing of these alloys e.g. casting and solution heat treatment, as well as during service e.g. decline in mechanical performance and alloy stability [1,3,4,5]. These issues, although known, have not been sufficiently quantified or understood.

A detailed and systematic study was therefore initiated to study the effects of Y and La additions on the properties of interest for turbine blade design. The study utilizes a common second generation single crystal nickel-base superalloy CMSX-4 as the base alloy, with the Y and La levels varied between approximately 20 ppm up to 350 ppm of combined Y+La content. Baseline CMSX-4 without Y and La additions were also included in the study for comparison. The as-cast material properties were studied in detail; in addition the effects of the Y and La additions on solution heat treatment and alloy stability were also examined.

Material

The nominal composition of CMSX-4 used in this study is as shown in Table I. Test bars approximately 12-13.5 mm diameter and 150 mm length were received in as-cast condition from Rolls-Royce plc. X-ray examination of the test bars indicated that the <001> was within 10° from the growth axis for all the bars used in this study. Note that the test bars were produced with non-optimized processing which resulted in relatively large primary dendrite arm spacing (PDAS) of up to 500 μm in most of the test bars, compared with more typical PDAS values of 200-300 μm in production components. The significantly larger PDAS of the test bars used in the current study are expected to have some effects on e.g. the solution heat treatment response, and concomitantly on related properties e.g. alloy stability.

Table I: Nominal Composition (wt. %) of Ni-base Superalloy CMSX-4, Balance Ni [1]

Al	Ti	Cr	Co	Mo	Hf	Ta	W	Re
5.6	1.0	6.5	9.6	0.6	0.1	6.5	6.4	3.0

The Y and La were added to the alloy ingot at the casting unit prior to melting [6]. After casting, the Y and La contents were noted to vary along a given test bar from the bottom to the top, with the bottom of the bar retaining higher Y and La levels. Utilizing this variation along selected test bars, a systematic variation in the Y and La contents with combined Y+La levels of approximately 20, 65 and 350 ppm were obtained. The Y and La concentrations were determined by utilizing acid digestion of the samples and measurement of the rare-earth levels with an inductively-coupled-plasma optical-emission-spectroscopy (ICP-OES) equipment at accredited laboratories. Note that the

CMSX® and CMSX-4® are registered trademarks of Cannon-Muskegon Corporation.

measurement accuracy of the Y and La concentrations associated with this measurement technique is typically ± 10%. In addition there may also be small variation in the Y+La levels within a particular area of the test bar, and between the test bars in which the Y+La levels were measured and the test bars which were used in the experiments. The Y+La levels indicated were obtained from measurements on multiple test bars (between 2-5) from a given mould, and in general within mould variation of the measured Y+La levels at a given height from the chill plate was within 10-15%.

Experimental

Microstructural Examination

Samples for microstructural characterization were cut normal to the <001> casting direction. Standard metallographic preparation techniques were used and at the final step the samples were fine-polished with colloidal silica suspension. Samples were examined using a Leica DMLM optical stereomicroscope. Where required, a Camscan MX2600 field-emission-gun scanning-electron-microscope (FEG-SEM) equipped with INCA EDX facility was utilised to examine the alloys in greater detail. The SEM was used with an accelerating voltage of 20 kV and a working distance of 10 mm to examine the microstructure in back-scattered electron imaging (BEI) mode and to carry out EDX analyses on chosen samples.

Electron-probe microanalysis (EPMA) X-ray mapping of the alloys in the as-cast condition was carried out to obtain a semi-quantitative measure of the degree of elemental micro-segregation in the as-cast materials. A Cameca SX100 instrument was used to carry out EPMA X-ray mapping. The beam conditions were 20 kV, 100 nA and the beam was fully focused (excitation volume for most X-rays in the alloy approximately 1-1.5 cubic microns). Areas of 750 μm × 750 μm were mapped at 1 μm resolution with a dwell time of 40 ms at each location. The following X-ray lines were used (the choice of lines is constrained by the need to avoid significantly overlapping lines):

Kα1	Al, Ti, Cr, Co
Lα1	Mo, W
Mα1	Hf, Ta
Mβ1	Re

All calibration standards were pure (99.999%) metals except for Al, for which pure synthetic corundum (Al_2O_3) was used. The analyzing crystals used were LiF (Cr, Co, W), LPET (Ti, Mo, Re), LTAP (Hf) and TAP (Al, Ta).

Differential Scanning Calorimetry (DSC)

The effects of Y and La additions on the thermal characteristics of the alloys, e.g. the solution heat treatment (SHT) window were investigated by carrying out DSC measurements on as-cast samples. A Netzsch DSC 404 equipment (by Netzsch-Gerätebau GmbH, Selb, Germany) was used where the sample holder has S-type thermocouples (Pt-Pt10%Rh) in both the sample and reference locations. The thermocouple in the sample location was calibrated against the melting temperatures of pure gold and pure nickel. Samples used for the DSC measurements are approximately 5 mm in diameter and 1.5 mm in height which were produced by electro-discharge machining (EDM). The samples were ground to remove EDM marks and finished to 4000-grit finish with SiC paper for the DSC runs. Alumina crucibles were used in all DSC experiments. All DSC runs were performed in a dynamic high purity argon environment with an argon flow rate of 50 mL min^{-1}. The heating rate was 20 K min^{-1} from room temperature to 600°C and thereafter 10 K min^{-1} up to 1450°C followed by cooling at 10 K min^{-1} from 1450°C to 1000°C.

All the DSC traces and thermal data presented in this study were from the heating portion of the DSC experiments to capture the thermal histories associated with the material and prior processing which determines the state of the material. The y-axes of the DSC traces presented were aligned with exothermic processes plotted in the positive y-direction.

Solution Heat Treatment (SHT) Trial

Solution heat treatment (SHT) trials were carried out to assess the potential of CMSX-4 with Y+La additions as a 'drop-in' upgrade to replace existing CMSX-4 in current engine components to capitalize on the benefits of the enhanced environmental protection performance of the alloy. Small-scale SHT trials were carried out in an AFT laboratory-scale vacuum furnace (by Advanced Furnace Technology, Cambridge, United Kingdom). The C-type controller thermocouple (W26%Rh-W5%Rh) was calibrated with an R-type thermocouple which has been calibrated against the melting temperature of pure gold. The reproducibility of the furnace temperature was within ± 1°C after the calibration. Samples of as-cast CMSX-4 test bars with Y+La additions were cut into 5-7 mm widths for the SHT trials. The SHT trials were carried out utilizing the conventional 1312°C/6hr CMSX-4 SHT cycle. After SHT run in the vacuum furnace, the samples were prepared for microstructural examination.

The area fractions of remnant interdendritic/incipient melting in the alloys with Y+La additions were quantified to assess the suitability of these alloys as 'drop-in' upgrade for the existing alloy. The samples were characterized in a 25-frame matrix arranged in a touching 5 × 5 array of 0.5 mm × 0.5 mm frames. The measurement technique did not distinguish between remnant interdendritic and incipient melting, therefore the area fraction data generated consist of the combined area fraction of remnant interdendritic and incipient melting.

Alloy Stability Studies

An assessment of the effects of Y and La additions on the phase stability of the alloy was also carried out. Samples were prepared from approximately 5 mm transverse section of as-solutioned test bars. Annealing was carried out at 1000°C and 1100°C with exposure times of up to 1000 hours. The annealing temperatures were chosen to replicate the temperatures experienced at various areas of the turbine blade during service, while the maximum annealing time was chosen to represent the approximate 'hot life-time' of the turbine blades. The annealing was carried out in Carbolite laboratory chamber furnaces in an air environment; after annealing the samples were removed from the furnace and left to cool in laboratory air. The samples were then prepared by polishing to finish with colloidal silica for examination in a Camscan MX2600 FEG-SEM operating at an accelerating voltage of 20 kV in BEI mode.

Samples were also deep-etched electrolytically in order to reveal the TCP phases in greater detail. The samples were polished to ¼ micron diamond finish and deep-etched using an electrolyte composed of 10% HCl and 1% tartaric acid in methanol. Samples were etched with an anodic current density of 2 mA/mm^2 for approximately 5 minutes and subsequently examined in a JEOL 5800LV SEM operating at an accelerating voltage of 20 kV in secondary electron imaging mode.

Preliminary investigation to identify the TCP phases was carried out by analyzing the selected area diffraction pattern (SADP) in a JEOL 200CX TEM operating at an accelerating voltage of 200 kV. Specimens for the TEM were electropolished using a 10% perchloric acid in methanol solution at -5°C temperature and 20 V potential difference. Samples were sectioned near the {011} plane; this way both the [111] and [001] poles are within reach using a double-tilt TEM sample holder and therefore the SADP of the phases associated with these poles could be analyzed.

Results

Microstructural Examination

An overview of the microstructures of as-cast CMSX-4 with Y+La additions is shown in Fig. 1. Dendrite cruciforms could be seen in both the 20 and 350 ppm materials. Minute bright phases residing mainly in the interdendritic areas were also observed. When the interdendritic areas of CMSX-4 with 350 ppm Y+La were examined in greater detail as shown in Fig. 2, in addition to γ and γ', two other distinct phases were also present. Firstly, one of the phases had an extremely bright contrast when imaged in BEI in the SEM; the areas associated with this phase were rich in Ta and Hf as determined with EDX analysis, on this basis this phase was presumed to be carbides. In addition, there were also areas observed with contrast slightly brighter c.f. the γ and γ' phases; these areas were associated with a different phase rich in Y and La as determined by EDX analysis. Both these phases were usually found adjacent to the coarse cellular γ' areas in the interdendritic region or adjacent to porosity; these areas of which represent the final areas to solidify during the casting process [7]. The size of most of these Y and La-rich phases in the 350 ppm Y+La material were up 10 μm in diameter. The bright phase rich in Ta and Hf was seen in the alloys for the range of Y+La additions investigated in this study, while the Y and La-rich phase were predominantly observed for materials with 350 ppm Y+La, becoming less frequent in the 65 ppm Y+La material and was rarely found in the 20 ppm Y+La material.

EPMA elemental maps of as-cast CMSX-4 with Y+La additions are shown in Fig. 3. The partitioning of the various major alloying elements was generally similar at the three different levels of Y+La additions. One of the observations from the EPMA maps is that at the three Y+La levels investigated, the concentration of Cr appears to be generally weaker in the interdendritic regions compared to the dendritic areas, however there is a peak in the concentration of Cr along certain edges of the interdendritic pools which is even beyond the concentration of Cr in the dendritic areas. The enrichment of Cr in these areas also appears to coincide with higher concentrations of Mo and Hf at these locations. These areas were the last areas to solidify during the casting process, where the remaining Cr, Mo and Hf solute rejected from the solid during solidification were concentrated into the remaining liquid during the terminal stages of solidification.

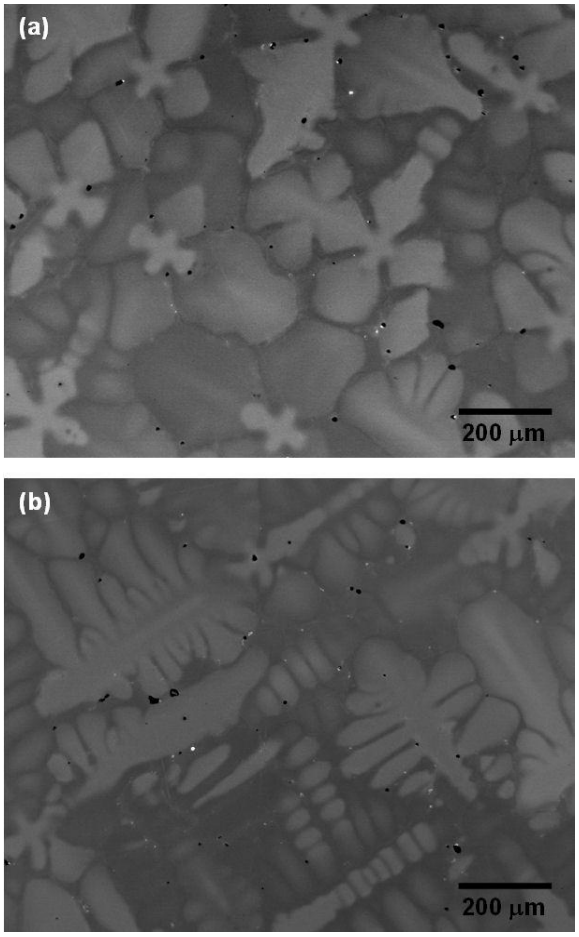

Fig. 1 BEI images showing an overview of the microstructure of as-cast CMSX-4 with Y+La additions (a) 20 ppm, (b) 350 ppm.

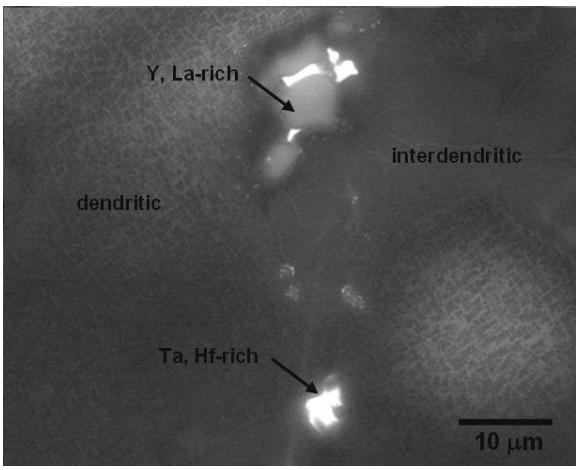

Fig. 2 Microstructure of inter-dendritic areas of as-cast CMSX-4 with 350 ppm Y+La additions.

(a)

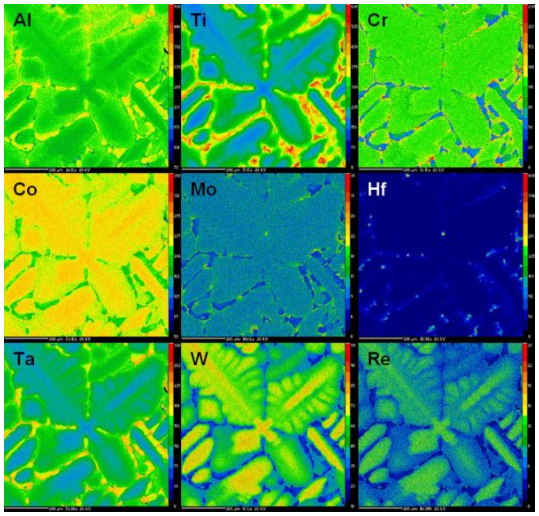

(b)

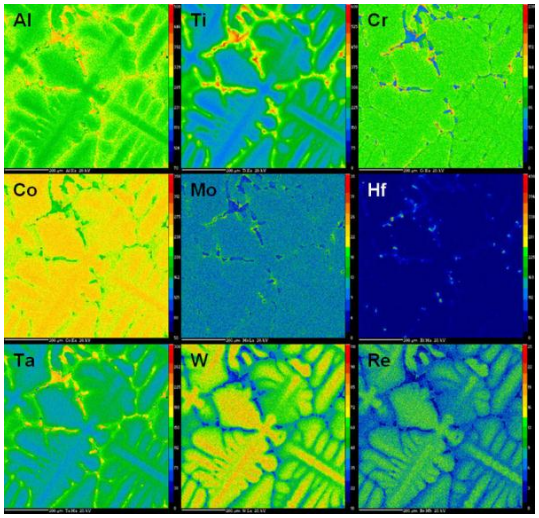

(c)

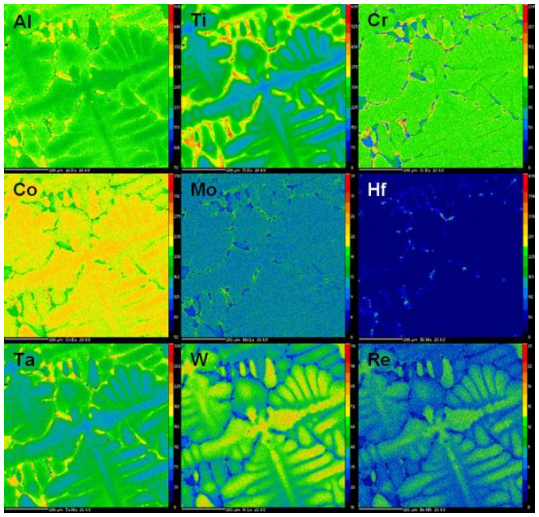

Fig. 3 EPMA maps of as-cast CMSX-4 with Y+La additions (a) 20 ppm, (b) 65 ppm, and (c) 350 ppm.

Differential Scanning Calorimetry (DSC)

The DSC traces and the first derivative plots (with respect to time) of these DSC traces i.e. *d*(DSC)*/dt* (the slope of the DSC traces) of baseline as-cast CMSX-4 as well as as-cast CMSX-4 with Y+La additions are shown in Fig. 4. Note that the DSC traces in Fig. 4(a) have been spaced out arbitrarily to better illustrate the effects of the Y and La additions on the thermal characteristics of the as-cast materials; therefore, heat flow values on the y-axis were relative rather than absolute. In Fig 4(a), two distinct (endothermic) peaks were observed on a given DSC trace when the sample is heated up to complete melting; the minor peak at lower temperature represents melting of the interdendritic areas while the larger peak denotes the melting of the bulk of the material. Incipient melting which is the first occurrence of localized melting in the interdendritic regions during heating up is denoted on the DSC trace as the point at which the relatively horizontal bulk solid line first exhibits an endothermic deviation from the tangent near the onset of the minor peak. In Fig 4(a), the DSC traces appear to show a progressive decreasing slope prior to the minor peak and the onset of the minor peaks could be seen to occur at progressively lower temperatures with increasing Y+La additions, which is indicative of the lowering of the incipient melting temperature (T_{IM}) with higher Y+La additions.

The T_{IM} was approximated by examining the *d*(DSC)*/dt*, plot, i.e. the temperature at which the *d*(DSC)*/dt* plot first show a significant change in its downward slope, corresponding to the very first moment of incipient melting (endothermic reaction) at the onset of the minor peak in the DSC trace. The T_{IM} of baseline as-cast CMSX-4 was approximated to be 1307°C; with Y+La additions, the T_{IM} appeared to be lowered to 1297°C for the three Y+La levels examined. However, on closer inspection of Fig. 4(b), the first derivative plots appear to be progressively shifted to lower temperatures (to the left) with increasing Y+La additions. This may be an indication that the T_{IM} is progressively lowered with increasing additions of Y+La, rather than a step-wise decrease of the T_{IM} to 1297°C for the range of Y+La levels investigated. The progressive decrease in T_{IM} was expected to be approximately 3°C with every step of the increase in Y+La level, i.e., from baseline, 20 ppm, 65 ppm down to approximately 1297°C for the highest Y+La level of 350 ppm.

Solution Heat Treatment (SHT) Trial

The microstructures of CMSX-4 with Y+La additions which have been subjected to the conventional CMSX-4 SHT cycle are shown in Fig. 5. Incipient melting and remnant interdendritic was not observed for CMSX-4 with 20 ppm Y+La. At 65 ppm Y+La, incipient melting was relatively rare although still occasionally visible, as shown by arrow in Fig. 5 (b). At the highest Y+La level of 350 ppm, significant degree of incipient melting was observed as shown in Fig. 5 (c).

The degree of incipient melting in the 65 and 350 ppm Y+La materials after SHT is shown in greater detail in Fig. 6. The 65 ppm Y+La material shows relatively rare incipient melting pools, while in the 350 ppm Y+La materials the degree of incipient melting was widespread. Note also in Fig. 6, the Y and La-rich phases could be observed in both the 65 and 350 ppm Y+La materials, very often adjacent to the incipient melted pools.

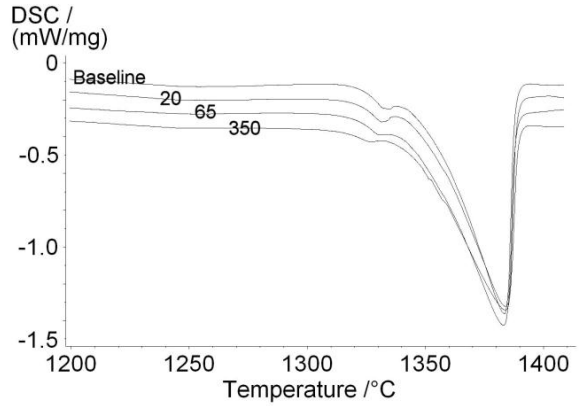

(a)

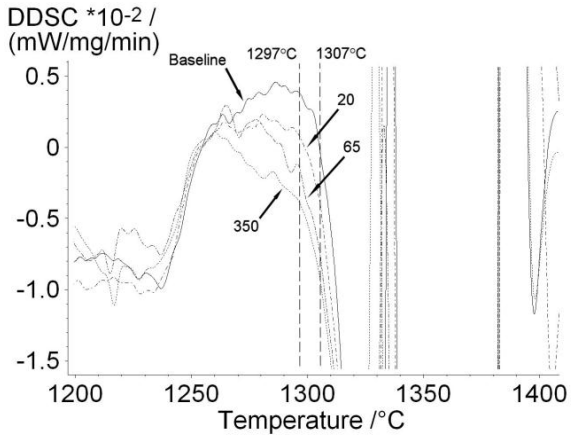

(b)

Fig. 4 DSC results of as-cast CMSX-4 with Y+La additions (a) DSC trace from heating portion of DSC experiments, (b) first-derivative (w.r.t. time) associated with DSC traces in (a).

The area fractions of remnant interdendritic/incipient melting in the SHT trial samples were 0.04%, 0.10% and 0.48% respectively for the alloys with 20, 65 and 350 ppm Y+La additions. The data replicates the degree of incipient melting in the samples as observed in Fig. 5. The area fraction of incipient melting appears low (<0.1%) when the Y+La level is kept at 65 ppm or below, which rises significantly to approximately 0.5% for the alloy with 350 ppm Y+La.

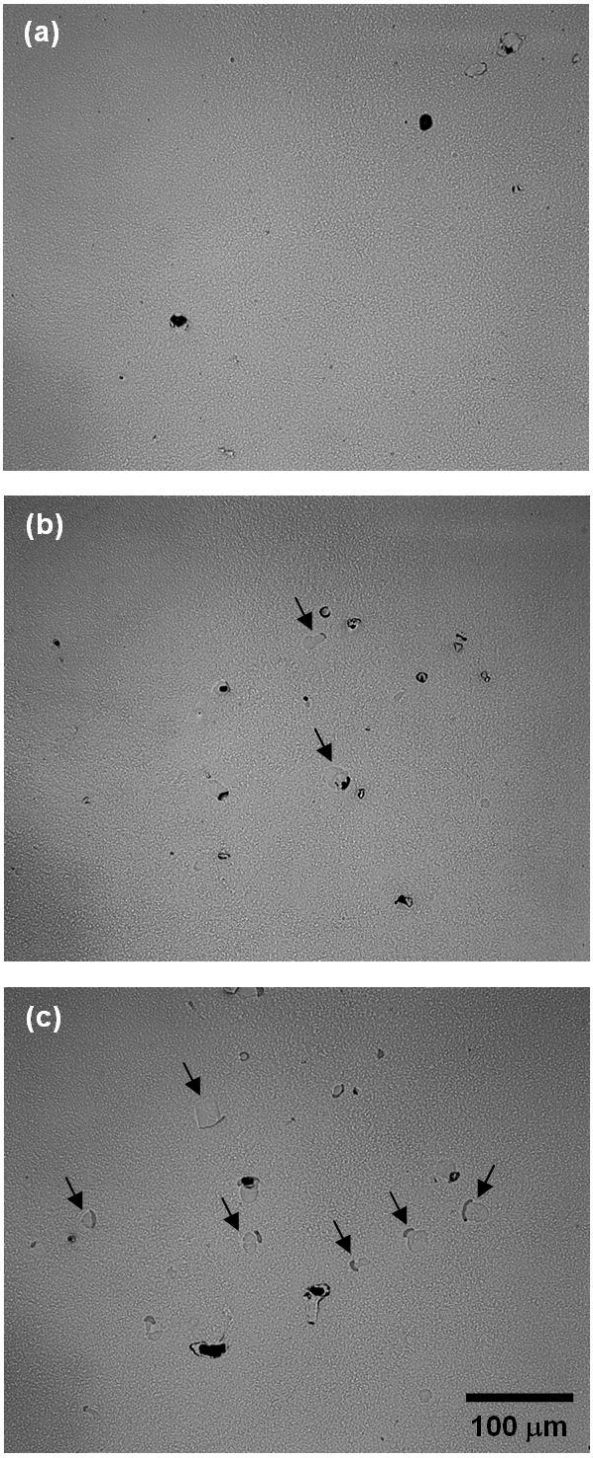

Fig. 5 CMSX-4 with Y+La additions after SHT at 1312°C/6hr (a) 20 ppm, (b) 65 ppm, and (c) 350 ppm.

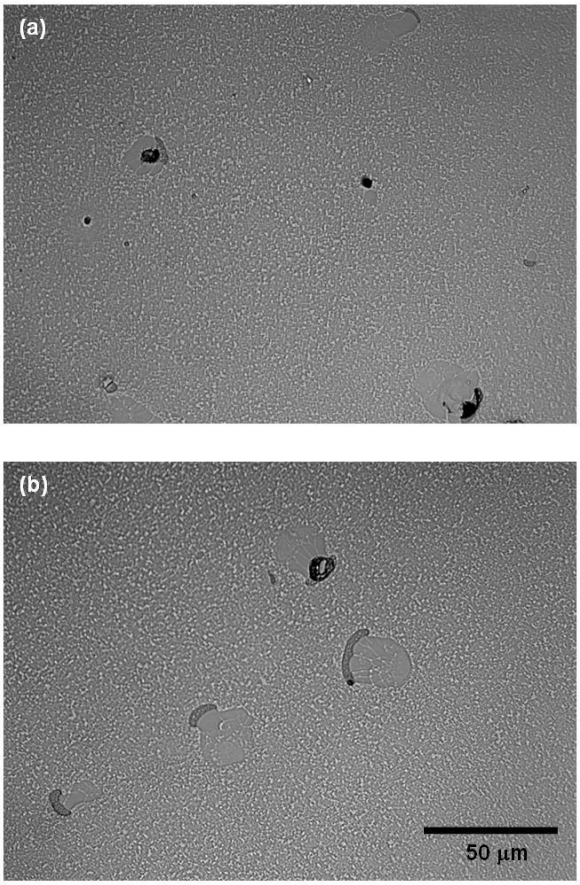

Fig. 6 Incipient melting in CMSX-4 with Y+La additions after SHT (a) 65 ppm, (b) 350 ppm.

Alloy Stability Studies

The microstructures of the alloys investigated after 1000 hours exposure at 1000°C and 1100°C are shown in Fig. 7. Note that these images represent amongst the worst areas in terms of TCP phase formation in the respective samples. For each alloy of a particular Y+La level, the severity of TCP phase precipitation increases with the higher exposure temperature of 1100°C. At a given exposure temperature, the propensity for TCP phase formation increases with increasing Y+La content up to 65 ppm, after which further increase in Y+La level to 350 ppm appears to cause a decrease in TCP phase formation. Note in Fig 7 (a) there were little or no TCP phases observed after 1000 hours exposure 1000°C in the 350 ppm Y+La material, the brighter phases observed are the Y and La-rich phase described earlier which are still mostly surrounded by incipient melted pools after the prolonged elevated temperature exposure. Note also from Fig. 7 that the TCP phases were formed mostly in the dendritic regions (e.g. in the 65 ppm Y+La materials after 1000hr at 1000°C although there were also occurrence of TCP phases forming at the boundaries between the dendrite arms and interdendritic regions (e.g. in the 20 ppm Y+La material after 1000hr at 1100°C).

The TCP phases formed in the CMSX-4 with Y+La additions are shown in greater detail in the deep-etched samples of the alloys which have been annealed at 1100°C for 1000 hours in Fig. 8. The type and morphology of TCP precipitates formed in the alloys appear relatively similar, however the quantity and relative proportions of the types of TCP phases were distinctly different. In the 20 ppm Y+La material, the TCP phases were of needle-like and thick plate-like morphology, while in the 65 ppm Y+La material, the TCP phases were observed to exhibit a combination of needle-like/fine whisker morphology and a thin plate-like morphology. Within the 65 ppm Y+La material, the needle-like/fine whisker TCP phases were more commonly observed compared to the thin plate-like TCP phases, and the overall amount of TCP phases observed in the 65 ppm Y+La material was distinctly higher compared to those observed in the 20 ppm Y+La material. Finally, in the 350 ppm Y+La material, the TCP phases which occurred in significantly lower quantity were mostly of the plate-like morphology, although the needle-like/fine whisker morphology was also occasionally observed.

Initial investigations carried out to identify the TCP phases indicate that the TCP phases were μ and R as shown in Fig. 9. These TCP precipitates were observed in the alloy with 65 ppm Y+La. The diffraction pattern inset in Fig. 9(a) is that of the μ phase near the $[\bar{1}10]_{\mu}$ pole with the $\langle 0001\rangle_{\mu}$ direction as indicated, while the diffraction pattern in Fig. 9(b) is that of the R phase near the $[\bar{1}10]_{R}$ pole with the $\langle 001\rangle_{R}$ direction as indicated.

Discussion

For the test bars used in the current investigation, within a given test bar the Y and La levels was noted to vary from the bottom to the top of the bar, with the bottom of the bar having higher Y and La content. This variation was due a variety of factors. The directional solidification casting process meant that the alloy remains molten in the ceramic shell for prolonged periods, with the bottom of the bar being the first to solidify. Losses are expected due to evaporation to the vacuum atmosphere under which the casting process is carried out. In addition, losses due reaction of Y and La with ceramic mould and cores are apparent [2,6]. In the current study, the effects of Y and La additions were investigated across the wide range of Y+La levels to encompass all possible scenarios which may be encountered in production and during service, given the complex geometries of turbine components.

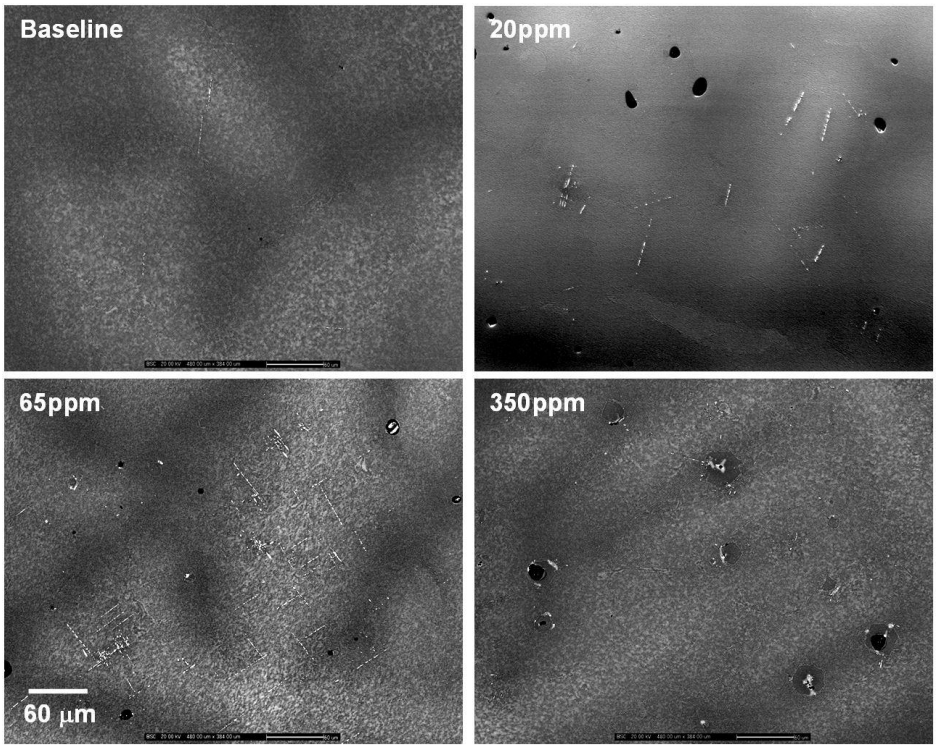

(a)

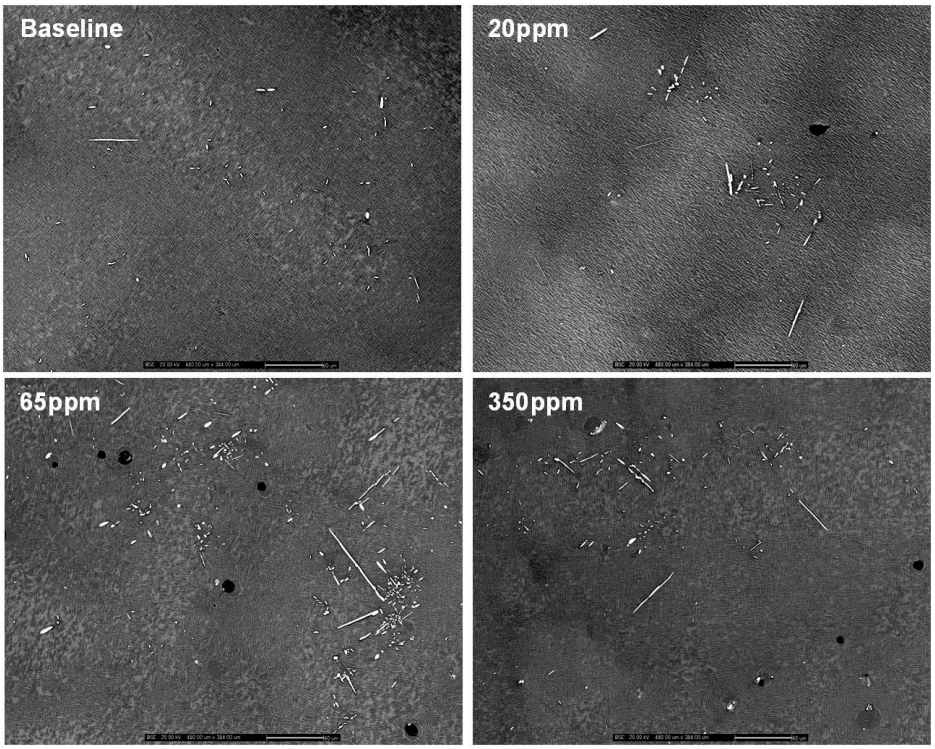

(b)

Fig. 7 Microstructure of CMSX-4 with Y+La additions after 1000 hours exposure at (a) 1000°C and (b) 1100°C

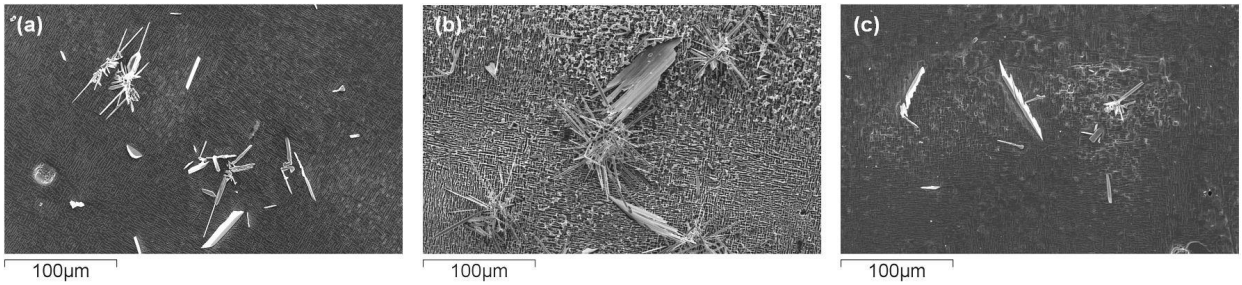

Fig. 8 Deep-etched microstructure of CMSX-4 with Y+La additions after 1000 hours exposure at 1100°C (a) 20 ppm, (b) 65 ppm, and (c) 350 ppm

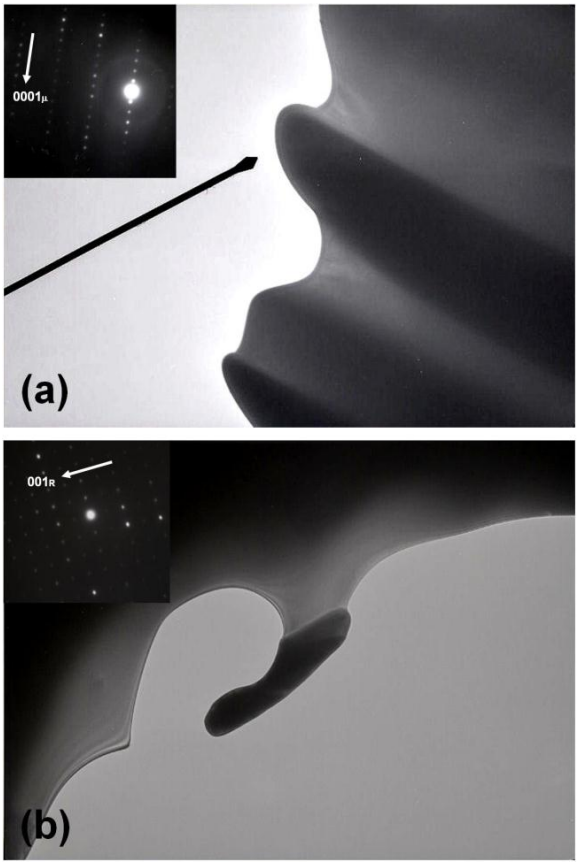

Fig. 9 TCP precipitates observed in CMSX-4 with 65 ppm Y+La (a) µ phase and (b) R phase.

In the as-cast condition, the high Y+La materials show the presence of Y and La-rich phases. These Y and La-rich phases were mostly observed in the interdendritic regions, adjacent to the coarse cellular γ' areas formed during the terminal stages of the directional solidification casting process [7]. These Y and La-rich phases are expected to be combinations of oxides, sulphides and/or oxysulphides of Y and La; in addition, in the materials with high Y+La contents, Ni-Y and Ni-La eutectics are also expected to be present [2,4,5,6,8,9]. Examination of the Ni-Y and Ni-La phase diagrams indicates that Y and La have no major solubility in Ni, and in addition most of the Ni-Y and Ni-La eutectics have relatively low melting points [2]. Recent chemical analyses carried out by the authors with laser-ablation inductively-coupled-plasma mass-spectrometry (LA-ICP-MS) do indeed show that the dendrite areas and most γ/γ' interdendritic areas are devoid of Y and La content; these results will also be reported in a future publication. The absence of Y and La in these areas meant that Y and La were continuously being rejected from the solid during solidification; hence were heavily segregated to the liquid in the terminal stages of solidification which explains the presence of Y and La-rich phases adjacent to the last interdendritic areas to solidify, and the small effect which the Y and La additions have on the solid/liquid partitioning of the major alloying elements as shown by EPMA elemental maps in Fig. 3. The low melting points of the Ni-Y and Ni-La eutectics also meant that these were the last phases to solidify after the solidification of the last γ/γ' interdendritic areas in the Y and La-containing alloys.

The absence of Y and La in the dendrite areas and most γ/γ' interdendritic areas also meant that the Y+La content as measured in the as-cast bulk analyses with ICP-OES were solely due to the Y and La tied up within the Y and La-rich phases. In addition, the sizes of these Y and La-rich phases were relatively similar in both the 65 and 350 ppm Y+La materials. Therefore to achieve higher Y+La content in the alloy, the frequency of these Y and La-rich phases are expected to be higher, which was indeed observed for the 350 ppm Y+La material compared to the 65 ppm material. It may also be expected that alloys with lower Y+La levels, e.g. the 20 ppm Y+La material, also has these Y and La-rich phases, however their size and/or frequency are expected to be much lower hence they were rarely observed during microstructural examination of the 20 ppm Y+La material.

The DSC results indicate only minor differences in the as-cast T_{IM} of the baseline alloy and the alloys with Y+La additions, the range of T_{IM} was approximately between 1297°C to 1307°C, where alloys with higher Y+La contents have lower T_{IM}. The minor difference in T_{IM} may be somewhat expected, since the elemental distributions of the major alloying elements were relatively similar as shown by EPMA of the as-cast materials. However, comparing the level of incipient melting observed after the SHT trials, the results were rather unexpected in light of the minor difference in T_{IM}.

During SHT, the ramp and soak steps were designed such that prior to reaching the soak at peak solution temperature, the ramp steps are significantly slowed down and the soak periods are more prolonged to allow the areas with the lowest melting

temperatures in the interdendritic regions to undergo homogenization, and in the process the local melting temperature is continuously raised. If the ramp and soak steps are too rapid, there will be insufficient time for homogenization of these low melting point areas to occur, leading to incipient melting during the ramp step itself or during the prolonged soak.

Comparing the degree of incipient melting observed after the SHT trials, the 350 ppm Y+La material show significantly greater susceptibility to incipient melting (~0.5% area fraction) compared to the 65 ppm Y+La material (approximately 0.1% area fraction). Yet there was only a minor difference between the T_{IM} of the 65 and 350 ppm Y+La materials, therefore the lowering of the T_{IM} with higher Y+La contents was unlikely to be the cause of such a large difference in the degree of incipient melting observed. This may be an indication that diffusion/homogenization of the interdendritic areas may be occurring differently with high levels of Y and La present.

Typically during SHT of alloys without Y and La additions, homogenization of the major alloying elements is occurring between the dendrite and γ/γ' interdendritic areas; the reduction in segregation leads to increases in local melting temperatures. In the as-cast materials with 65 and 350 ppm Y+La, the presence of Y and La-rich phases was observed in the interdendritic areas. After SHT, these Y and La-rich phases were still observed, i.e. they were not dissolved during prolonged exposure at elevated temperatures due to lack of major solubility of Y and La in Ni. It was noted that incipient melting was very frequently observed adjacent to these Y and La-rich phases after SHT, therefore these Y and La-rich phases must be playing a critical role in inducing the incipient melting. The Y and La-rich phases have been speculated to be combinations of oxides, sulphides and/or oxysulphides of Y and La, as well as Ni-Y and Ni-La eutectics. The oxides, sulphides and oxysuphides of Y and La are relatively stable and have relative high melting points, hence relatively unaffected by SHT temperature; the Ni-Y and Ni-La eutectics on the other hand have much lower melting points, therefore these may be in an entirely liquid state at the elevated temperatures during SHT. At these elevated temperatures, local diffusion of Y and La from the Ni-Y and Ni-La eutectic phases into the surrounding dendrite and γ/γ' interdendritic areas may be occurring due to the high concentration gradients between these eutectic phases and the surrounding areas devoided of Y and La in the as-cast condition. As the concentration of Y and La builds up in the dendrite and γ/γ' interdendritic areas surrounding these eutectic phases, it may have the effect of lowering the local melting temperature of these areas, leading to incipient melting as the SHT progresses. There are some recent work by the authors, where incipient melting was not seen when the as-cast 350 ppm Y+La material was heat-treated at 1295°C for 3 hours, but after prolonged exposure at 1295°C for 24 hours, incipient melting was observed. The observation of incipient melting with the prolonged 24 hours exposure would support the argument that Y and La diffusion from the Y and La-rich eutectic phases into surrounding areas is lowering the local melting point; with the prolonged exposure, higher concentrations of Y and La would be expected in the areas surrounding these eutectic phases, causing a greater decrease in the local melting temperature to even below the exposure temperature of 1295°C, giving rise to the incipient melting observed. In such case where the T_{IM} is continuously decreased with longer elevated temperature exposure, there may be a need to balance the SHT time to achieve sufficient homogenization and dissolution of the interdendritic areas while minimizing the degree of incipient melting within the SHT time. The CMSX-4 with Y+La additions used in the current study were also cast with non-optimized casting parameters resulting in much larger PDAS than those typical of production components. It is expected that with optimized processing, smaller PDAS may lead to shorter diffusion lengths and consequently improved homogenization during SHT.

In terms of alloy stability, the types of TCP phases formed at different Y+La levels were relatively similar and this suggests that the mechanisms of TCP phase formation may be similar at the various Y+La levels. The quantity of plate-like TCP phase does not appear vastly different at the three Y+La levels, however the plate-like TCP phase in the 65 ppm Y+La material appears thinner although generally greater in surface area. The plate-like TCP phase in the 20 and 350 ppm Y+La materials generally appeared thicker compared to the plate-like TCP phase in the 65 ppm Y+La material. In terms of the fine whisker/needle-like TCP phase, the quantity builds up from 20 ppm Y+La up to a maximum in the 65 ppm Y+La material, but was greatly diminished in the 350 ppm Y+La material. Both these trends leads to the greatest amount of TCP phases being observed in the 65 ppm Y+La material. The proportion of the needle-like/fine whisker TCP phase was also significant higher compared to the plate-like TCP phase in the 65 ppm Y+La material.

The TCP phases were generally observed in the dendritic areas and at boundaries between dendrite arms and interdendritic areas. Formation of TCP phases in dendritic areas has been commonly reported in the literature, due to segregation of TCP-forming elements e.g. Re and W to the dendrite during solidification. The elemental segregation could not be completely eliminated during SHT, therefore residual segregation and consequently higher concentrations of TCP-forming elements in the dendrite areas lead to greater propensity of TCP phase formation in these areas. With regard to TCP phases which were observed at the boundaries between dendrite arms and interdendritic areas, this was due to enrichment of Cr, Mo and Hf in the last interdendritic areas to solidify during casting of the materials used in this study as shown by EPMA maps of major alloying elements. The enrichment may also cause residual segregation of these elements which could not be completely eliminated even after SHT. All these three elements, especially Cr and Mo have been persistently linked to increased propensity to TCP phases formation in literature [10].

There was very limited information in the literature pertaining to the effects of Y and La additions on the propensity and type of TCP phase formation in Ni-base superalloys. The images in Fig. 7 represent the worst areas in terms of TCP phases formation, and there were quite apparent differences between the amount of TCP phases formed in the baseline alloy and in the Y and La-containing alloys. The Y and La additions therefore do appear to have an apparent and real effect of increasing the propensity of TCP phase formation compared to the baseline alloy. However, on the contrary, when examining the effects of Y+La levels on the propensity of TCP phase formation, there is an increase in the TCP phases formed with Y+La additions up to 65 ppm, after which the TCP phases formed appeared to decrease at the higher Y+La levels of 350 ppm. If Y and La does contribute to TCP

phase formation, the amount of TCP phases formed should increase with increasing levels of Y+La additions, with the highest amount of TCP should be seen in the 350 ppm material, however this was not observed in the experiments.

The Y and La have been mentioned to occur very locally in the Y and La-rich phases in the interdendritic regions last to solidify, yet it has a somewhat surprising effect of increasing the TCP phases formed in the dendrite areas and at the edges between the dendrite and interdendritic areas in the Y and La-containing alloys. Recent chemical analyses with LA-ICP-MS on solutioned samples (as used for the alloy stability studies) indicate that there is a residual Y and La content in the dendrite and interdendritic γ/γ' areas after SHT; the level of Y and La appears to be saturated at very low and constant levels of Y and La irrespective of the bulk Y+La levels in the alloys. However, the amount and type of TCP phases formed in the dendritic and interdendritic areas for the three levels of Y+La investigated were relatively different. Clearly the effects of Y and La additions on TCP phase formation were much more complicated. The mechanism by which Y and La enhances formation of TCP phases remains unclear, however it is expected that the TCP phase formation is extremely sensitive to the local Y and La contents, which is governed by the frequency of local occurrence of the Y and La-rich phases. Further work is required to gain better understanding of the underlying mechanisms of TCP phases formation in the Y and La-containing alloys which would hopefully also clarify the effects of Y and La additions of the propensity and type of TCP phases formed.

Summary and Conclusions

A systematic study on the effects of Y and La additions on the processing and properties of a second generation single crystal nickel-base superalloy CMSX-4 has been carried out. The outcome of the study could be summarized as follows:

- In both the as-cast and solutioned conditions, Y and La occurred very locally in the form of Y and La-rich phases. These phases were primarily observed in materials with Y+La levels of 65 and 350 ppm, possibly due to the increased frequency of these phases at higher Y+La levels.
- Y and La additions did not appear to have significant effect on the partitioning of the major alloying elements as shown by EPMA elemental maps.
- the as-cast incipient melting temperatures of CMSX-4 were progressively lowered with increasing levels of Y+La additions; the change may be up to 10°C between baseline CMSX-4 and CMSX-4 with 350 ppm Y+La.
- CMSX-4 with Y+La levels of up to 65 ppm shows a low degree of incipient melting ($\leq$0.1% total area fraction) when subjected to the conventional CMSX-4 SHT cycle, At 350 ppm Y+La, significant incipient melting was observed (~0.5% total area fraction)
- Y and La additions caused an increased propensity to TCP phases formation in CMSX-4 after 1000 hours exposure at 1000°C and 1100°C. The propensity to TCP phases formation increases with Y+La additions up to 65 ppm, which appeared to decrease at the higher Y+La level of 350 ppm.

The results of this study highlight the need to carefully balance the advantages and disadvantages associated with the additions of Y and La to Ni-base superalloys. The improvement which may be obtained in environmental protection performance should be carefully weighed against various potential detrimental issues. In the current study these were in the forms of solution heat treatment and alloy stability, both which may have further detrimental effects on other properties, e.g. elevated temperature fatigue and creep performance.

Acknowledgement

The authors would like to acknowledge the support of Professor A.L. Greer at the Department of Materials Science and Metallurgy for the provision of facilities and Rolls-Royce plc. through the Rolls-Royce UTP at the University of Cambridge for the provision of materials and funding. Funding from EPSRC under the Rolls-Royce plc. Strategic Partnership (Grant EP/H500375/1) were also gratefully acknowledged. The authors also wish to express appreciation to Dr. Robbie A. Hobbs (previously at Rolls-Royce plc.), Dr. Brian Cooper at Precision Casting Facility, Rolls-Royce plc., Dr. Chiara Petrone (previously at Dept. of Earth Sciences, University of Cambridge) and Mr. Kevin Roberts of the Dept. of Materials Science and Metallurgy, University of Cambridge for assistance during various experiments carried out in the study.

References

1. K. Harris and J.B. Wahl, Superalloys 2004, TMS (2004), 45-52.
2. D.A. Ford, K.P.L. Fullagar, H.K.Bhangu, M.C. Thomas, P.S. Burkholder, P.S. Korinko, K. Harris and J.B. Wahl, J. Eng. Gas Turbines Power, 121 (1999), 138-143.
3. M.C. Thomas, R.C. Helmink, D.J. Fraiser, J.R. Whetstone K. Harris, G.L. Erickson, S.L. Sikkenga and J.M. Eridon, in Materials For Advanced Power Engineering 1994, Part II (1994), 1075-1098.
4. M. Marchionni, D. Goldschmidt and M. Maldini, Superalloys 1992, TMS (1992), 775-784.
5. Y.F. Han and C.B. Xiao, Intermetallics, 8 (2000), 687-691.
6. P.R. Aimone and R.L. McCormick, Superalloys 1992, TMS (1992), 817-823.
7. H.T. Pang, H.B. Dong, R. Beanland, H.J. Stone, C.M.F. Rae, P.A. Midgley, G. Brewster, and N. D'Souza, Metall. Mater. Trans. A, 40A (2009), 1660-1669.
8. A. Kumar, M. Nasrallah and D.L. Douglas, Oxidation of Metals, 8 (1974), 227-263
9. K. B. Povarova, A. A. Drozdov, N. K. Kazanskaya, A. E. Morozov, Yu. R. Kolobov, T. N. Vershinina, and E. V. Kozlov, Russian Metallurgy (Metally), 2008 (2008), 398–405.
10. C.M.F. Rae and R.C. Reed, Acta Mater, 49 (2001), 4113–4125